

Ferromagnetism induced by strains in Pd nanoparticlesY. Oba,^{1,*} T. Sato,¹ and T. Shinohara²¹*School of Integrated Design Engineering, Graduate School of Science and Technology, Keio University, 3-14-1 Hiyoshi, Kohoku-ku, Yokohama, Kanagawa 223-8522, Japan*²*Japan Atomic Energy Agency, 2-4, Shirakata, Tokai, Ibaraki 319-1195, Japan*

(Received 10 July 2008; revised manuscript received 9 October 2008; published 22 December 2008)

The origin of the ferromagnetism that appears in the core region of Pd nanoparticles is discussed. According to many previous theoretical calculations, the onset of this ferromagnetism is closely related to the crystal structure and defects. In order to consider the contribution of crystal structure to the appearance of ferromagnetism in the Pd nanoparticles, we performed x-ray diffraction experiments and Warren-Averbach analysis. The results revealed that the standard deviation of strain $\Delta\varepsilon$ showed a positive correlation with the saturation magnetization, with the ferromagnetism appearing when $\Delta\varepsilon$ became larger than about 0.5%. This suggests that the strains induce internal ferromagnetism in the Pd nanoparticle. Compared to the critical magnitude of the strain at which ferromagnetism is predicted by the theoretical calculations, however, the estimated $\Delta\varepsilon$ is too small to explain the origin of ferromagnetism. Therefore, the strains smaller than the theoretical predictions should also give rise to the ferromagnetism or the strains should contribute to the magnetism not only through lattice expansion but also through changes in the crystal symmetry.

DOI: [10.1103/PhysRevB.78.224417](https://doi.org/10.1103/PhysRevB.78.224417)

PACS number(s): 75.50.Tt

I. INTRODUCTION

Magnetic materials on the nanoscale have been intensively studied in connection with the recent progress in information technology and the need for high-density magnetic storage media. In the nanometer range, magnetic properties are significantly affected by size effects; then exotic features often occur. Recently, the appearance of ferromagnetism in nanoparticles of transition metals which have no magnetic ordering in bulk has been reported.¹⁻⁶ Understanding the origin of the ferromagnetism is a fundamental issue and also produces a practical perspective in that the preparation of nanoparticles is useful to control magnetism even in materials usually known as nonmagnetic. In the investigation of fundamental magnetism, nanoparticles have some advantages; e.g., substrates, which influence the physical properties through the hybridization of electron orbits, are not necessary, and thus neither mismatching of lattice constants nor interdiffusion between target and substrate atoms occurs. Therefore, the intrinsic magnetism on the nanoscale can be observed using nanoparticles.

Pd is magnetically sensitive to external influences such as substrates because it has a large electron density of states (DOS) at Fermi energy and a sharp $4d$ peak of energy-dependent DOS just below the Fermi energy.^{7,8} We have discovered the appearance of ferromagnetism in free-standing Pd nanoparticles.² The ferromagnetism in these nanoparticles had two components; i.e., the ferromagnetism appearing on the surface and that in the core region. The surface ferromagnetism disappeared by the adsorption of oxygen gas, while the internal ferromagnetism was not affected by the surface condition of the nanoparticles.^{3,9} In these previous studies, the surface ferromagnetism was primarily focused because the internal ferromagnetism was comparatively small. In the present study, however, we found different magnetic behavior in some sample, where the internal ferromagnetism was as large as the surface ferromagnetism. The previous reports

already elucidated that the origin of the surface ferromagnetism was attributed to the two-dimensional character of the particle surface.^{2,3,9} In contrast, the origin of the internal ferromagnetism has not been clarified yet.

Thus, we focused on the effects of crystal structure and defects on the internal ferromagnetism in this report because a lot of theoretical research has predicted that these effects induce ferromagnetism in Pd and that the crystal defects are insensitive to the surface condition.^{7,8,10-15} Provided that the changes in crystal structure and defects satisfy the Stoner criterion of ferromagnetism, Pd should show ferromagnetic ordering in the picture of itinerant magnetism. In addition, some experimental studies have pointed out that crystal defects were possible causes of the ferromagnetism of Pd nanoparticles.^{4,9}

From the analysis of x-ray diffraction (XRD) profiles, the amounts of various crystal defects, e.g., strain, stacking faults, and twin boundaries, can be estimated.¹⁶⁻¹⁹ In order to clarify the origin of the internal ferromagnetism in connection with the crystal structure and defects, we performed a detailed analysis of XRD and magnetic data of Pd nanoparticles.

II. EXPERIMENTAL PROCEDURE

Pd nanoparticles were prepared by the gas-evaporation method in Ar gas. The initial vacuum was $\sim 10^{-7}$ Pa. High-purity Pd powder (Johnson Matthey Co., Ltd., 99.998%) was evaporated from an electrically heated W boat (purity 99.99%) into Ar gas of ~ 100 Pa purified by gas filters (H_2 , O_2 , and $\text{H}_2\text{O} \leq 1$ ppb). The experimental details have been described elsewhere.² For the observation of the particle size and shape, a FEI TECNAI F20 transmission electron microscope (TEM) was used. The XRD measurement of Pd nanoparticles was performed by a RIGAKU RAD-C diffractometer using $\text{Cu } K\alpha$ radiation. The magnetic data were obtained using a commercial superconducting quantum inter-

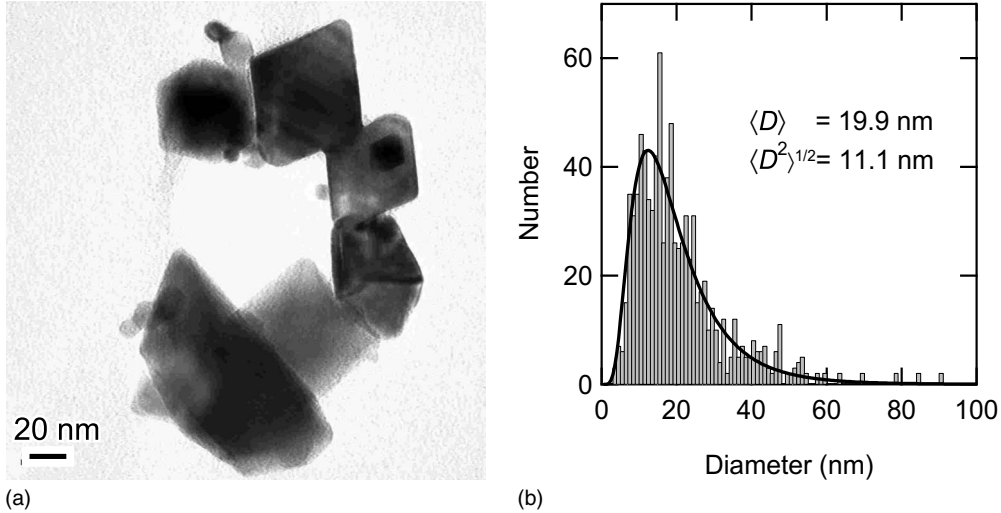


FIG. 1. Typical TEM image of Pd nanoparticles in (a). Histogram of the Pd nanoparticles with $\langle D_{\text{TEM}} \rangle$ of 19.9 nm and ΔD_{TEM} of 11.1 nm in (b). Solid line shows the logarithmic-normal fitting discussed in the text.

ference device (SQUID) magnetometer (Quantum Design MPMS-5). The sample was put in a quartz tube for the magnetic measurement. To limit the detection to internal ferromagnetism only, the samples were exposed to a sufficient amount of O_2 gas to suppress the surface ferromagnetism prior to the magnetic measurement.^{3,9} Therefore, we could focus on just the internal magnetism.

The XRD profiles were corrected with the Lorentz polarization factor and Debye-Waller factor to evaluate the true 2θ dependence. The instrumental function was deconvoluted by the Stokes method using LaB_6 powder as a standard. Strain ε is defined as $\varepsilon = (d\{hkl\}_{\text{nanoparticle}} - d\{hkl\}_{\text{bulk}}) / d\{hkl\}_{\text{bulk}}$, where $d\{hkl\}_{\text{nanoparticle}}$ and $d\{hkl\}_{\text{bulk}}$ are the $\{hkl\}$ plane spacings in nanoparticles and bulk material, respectively. We evaluated the average of strain $\langle \varepsilon \rangle$ from the shifts of diffraction lines. The stacking fault probability α , which is defined in terms of the probability that a given crystal plane contains a stacking fault, was also determined based on the line shift.^{18,19}

Warren-Averbach (W-A) analysis was then performed to estimate the standard deviation of strains $\Delta\varepsilon = ((\varepsilon - \langle \varepsilon \rangle)^2)^{1/2}$ from the broadening of the Bragg peaks.^{16,17} This method can distinguish between the broadening due to strain and that due to particle diameter. $\Delta\varepsilon$ generally represents the standard deviation of strains randomly oriented in samples; the dependence of $\Delta\varepsilon$ on crystal orientation was evaluated using two sets of diffraction lines, i.e., $\{111\}$ – $\{222\}$ and $\{200\}$ – $\{400\}$ lines, which correspond to $\langle 111 \rangle$ ($\Delta\varepsilon_{\langle 111 \rangle}$) and $\langle 100 \rangle$ ($\Delta\varepsilon_{\langle 100 \rangle}$) orientations, respectively. The twin boundary probability β was also estimated using these sets of diffraction peaks,¹⁸ where β is the probability of the appearance of twin boundaries similar to α . In addition, the average particle diameter was evaluated from the broadening due to particle size.

III. RESULTS AND DISCUSSION

A typical image and the size distribution of samples obtained by TEM are shown in Fig. 1. The Pd nanoparticles

were well-defined polyhedrons composed of octahedrons and multiple twins.^{20,21} In such polyhedrons, the particle diameter cannot be exactly determined. Thus, we used the distance between the opposite apexes or edges D_{TEM} as the characteristic size of a nanoparticle. We obtained an average of the characteristic sizes $\langle D_{\text{TEM}} \rangle$ and a standard deviation ΔD_{TEM} by logarithmic-normal fitting to the histogram of measured diameters for each sample as shown in Table I. A large distribution of particle sizes of the Pd nanoparticles was observed.

The XRD profile of the Pd nanoparticles clearly showed eight sharp peaks corresponding to those of bulk Pd [Fig. 2(a)]. The eight lines were labeled by Miller indices in Fig. 2(a), as referring to the XRD profile of bulk Pd crystal. The intensity ratio of the diffraction lines in the nanoparticles scarcely differed from that in bulk. The linewidths were different and the peak positions were slightly different among the nanoparticle samples. Figure 2(b) shows the $\{111\}$ diffraction line of each sample as an example. The intensity is normalized by the maximum value. The line position is adjusted so that each center is equal to zero. As a result of the XRD measurements, the lattice structure of the nanoparticles was identified with the fcc structure of bulk Pd. The difference of the linewidths among the nanoparticle samples reveals that the particle size and/or the amounts of the lattice defects in the samples differ from each other.

In order to discuss the correlation between the magnetism and lattice defects in detail, we estimated the magnitude of lattice defects and particle diameter based on the XRD profile using the W-A method as shown in Table I. To ensure accurate results, the average particle diameter $\langle D_{\text{W-A}} \rangle$ estimated from the W-A method was compared with $\langle D_{\text{TEM}} \rangle$. Figure 3 shows $\langle D_{\text{W-A}} \rangle$ as a function of $\langle D_{\text{TEM}} \rangle$. The monotonic relation between $\langle D_{\text{W-A}} \rangle$ and $\langle D_{\text{TEM}} \rangle$ indicates that the two parameters are essentially identical. This supports the accuracy of our XRD analyses. However, the magnitude of $\langle D_{\text{W-A}} \rangle$ insufficiently agrees with that of $\langle D_{\text{TEM}} \rangle$. This is partially because $D_{\text{W-A}}$ is the particle diameter, and D_{TEM} has the characteristic size described above.

TABLE I. Values of crystal defects in Pd nanoparticles.

	Sample 1	Sample 2	Sample 3	Sample 4	Sample 5
$\langle \varepsilon \rangle$ (%)	-0.09 ± 0.32	-0.05 ± 0.34	-0.10 ± 0.31	-0.15 ± 0.39	-0.1 ± 1.5
$\Delta \varepsilon$ (%)	0.50 ± 0.33	0.76 ± 0.04	0.85 ± 0.02	1.11 ± 0.06	1.34 ± 0.41
$\Delta \varepsilon_{100}$ (%)	0.00 ± 0.00	0.90 ± 0.05	0.89 ± 0.04	0.49 ± 0.15	1.79 ± 0.13
$\Delta \varepsilon_{111}$ (%)	0.44 ± 0.31	0.58 ± 0.40	1.44 ± 0.08	0.75 ± 0.04	0.00 ± 0.00
α (%)	0 ± 2	0 ± 2	0 ± 2	0 ± 1	0 ± 7
β (%)	1 ± 4	1 ± 4	1 ± 4	0 ± 2	2 ± 10
$\langle D_{W-A} \rangle$ (nm)	22.1 ± 0.2	30.8 ± 3.8	25.8 ± 0.3	24.7 ± 0.1	24.1 ± 0.5
$\langle D_{TEM} \rangle$ (nm)	19.9 ± 0.6	34.1 ± 1.3	31.0 ± 3.6	30.0 ± 2.0	23.9 ± 2.0
ΔD (nm)	11.1 ± 0.7	27.2 ± 2.5	30.1 ± 8.6	27.0 ± 4.3	17.2 ± 3.5
M_s (emu/g)	0.030 ± 0.009	0.294 ± 0.001	0.392 ± 0.005	1.035 ± 0.005	1.152 ± 0.012

The values of $\langle \varepsilon \rangle$, α , and β were almost zero within the error. Comparatively large values of $\Delta \varepsilon$, $\Delta \varepsilon_{100}$, and $\Delta \varepsilon_{111}$ were observed in the present samples, although their magnitudes had a wide distribution, where $\Delta \varepsilon$ denotes the standard deviation in the distribution of all kinds of strains in a sample, and $\Delta \varepsilon_{100}$ and $\Delta \varepsilon_{111}$ represent those of the strains oriented along the $\langle 100 \rangle$ and $\langle 111 \rangle$ directions, respectively. The negligibly small value of $\langle \varepsilon \rangle$ indicates that both the positive and negative strains equally exist in nanoparticles. In addition, there was no apparent correlation among $\Delta \varepsilon$, $\Delta \varepsilon_{100}$, and $\Delta \varepsilon_{111}$. This indicates that the strains were randomly oriented in the samples.

The characteristic of the standard deviation of strain, i.e., the large value of $\Delta \varepsilon$ in contrast to the negligibly small $\langle \varepsilon \rangle$, can be consistently interpreted from the following viewpoint. First, the present sample preparation method probably contributed to the increase in the amount of strain. The nanoparticles were grown by the condensation of Pd vapor, which is a nonequilibrium process. Thus, the nanoparticles possibly include the high-energy states in which the crystal defects are stabilized. Next, in the freestanding nanoparticle with ~ 10 nm the total energy is typically composed of cohesive

energy, surface energy, and energy of crystal defects.²⁰ In such a nanoparticle, the contribution of the surface energy should be pronounced due to the large ratio of the surface area to volume. In addition, the energy of crystal defects is also important because the formation of crystal defects is often accompanied by the reduction in surface energy through the reduction in total surface area, as observed in the multiply twinned particles. Thus, the nanoparticle easily contains crystal defects. A theoretical study²⁰ indicated that some multiply twinned particles inherently contain inhomogeneous strains even in their stable state, i.e., the crystal lattice contracts radially (negative strain) and expands circumferentially (positive strain). On the other hand, the absence of $\langle \varepsilon \rangle$ should reflect the high stability of the lattice constant in bulk Pd. It is worth noting that the Pd nanoparticle with a diameter of ~ 10 nm prepared by the inert gas-evaporation method contained small $\langle \varepsilon \rangle$ as reported by Reimann and Würschum.²² Consequently, we can propose the picture that the present Pd nanoparticles basically prefer the bulk crystal structure and the expansion and contraction of the crystal lattice are concurrently induced so as to decrease the surface energy.

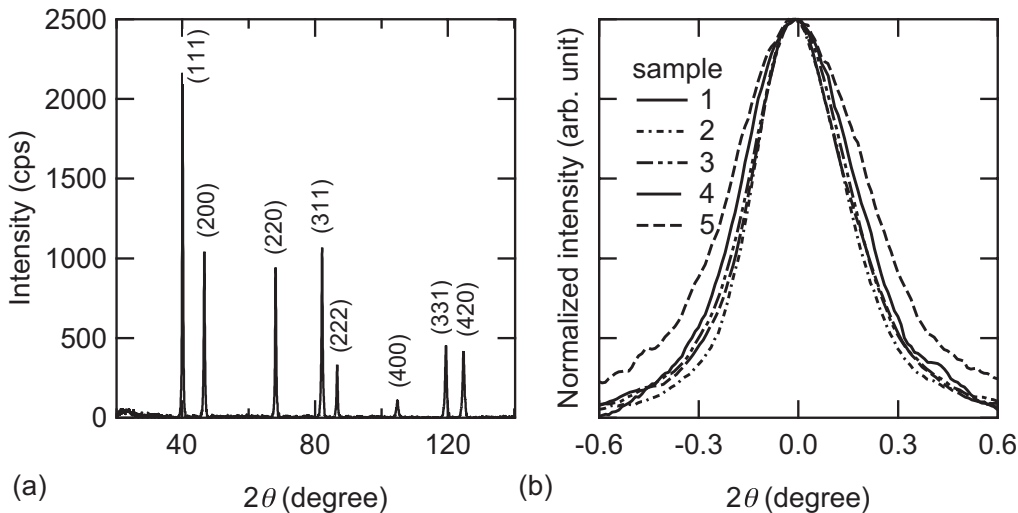


FIG. 2. Typical XRD profile of the Pd nanoparticles with $\langle D_{TEM} \rangle$ of 30.0 nm in (a). The normalized $\{111\}$ diffraction lines of all samples in (b).

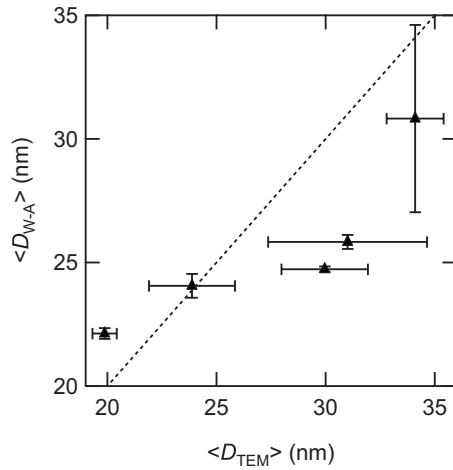


FIG. 3. $\langle D_{W-A} \rangle$ as a function of $\langle D_{TEM} \rangle$. The broken line shows the relation $\langle D_{W-A} \rangle = \langle D_{TEM} \rangle$.

The magnetization of the Pd nanoparticles consisted of a saturation component and a paramagnetic component linearly dependent on a magnetic field (the details of the magnetic properties were reported in Refs. 2 and 9). According to the previous study,² this corresponds to the coexistence of ferromagnetism and paramagnetism in a nanoparticle, i.e., part of the nanoparticle is ferromagnetic and the other part remains paramagnetic, as in bulk Pd. Since the surface atoms are probably covered with air, the ferromagnetic component is regarded as only the internal ferromagnetism. The magnitude of the internal ferromagnetism is same order as that of the surface ferromagnetism.² To discuss only the ferromagnetism of nanoparticles without uncertainty arising from the background, we fitted the magnetization curve obtained in magnetic fields higher than 2 T by a linear function and estimated the saturation magnetization M_s from the extrapolation of the fitting line to a zero field. The values of M_s , observed in Fig. 4, are significantly different among the samples although the temperature-dependent features are qualitatively similar. M_s in all samples is scarcely temperature dependent below 300 K, and thus the Pd nanoparticles probably have blocking temperature sufficiently higher than

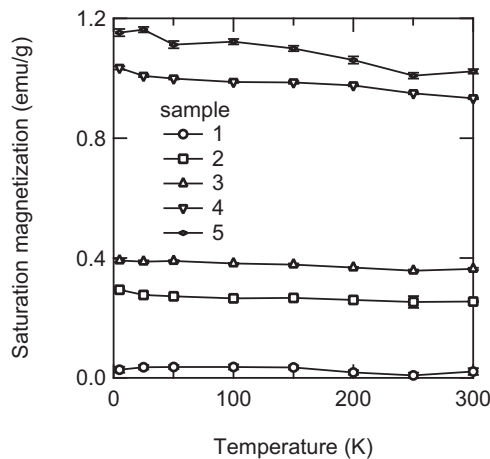


FIG. 4. Temperature dependence of M_s in all the samples.

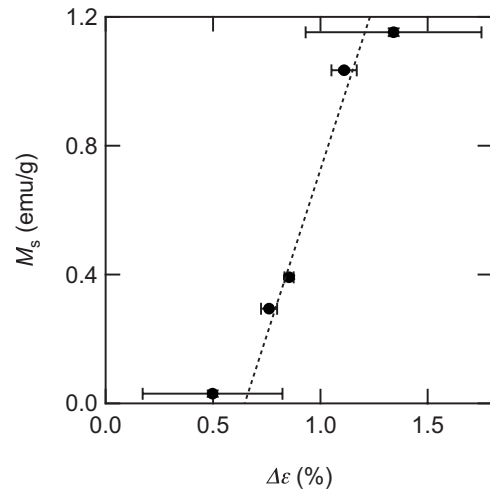


FIG. 5. M_s as a function of $\Delta \epsilon$. The broken line shows the linear fitting discussed in the text.

room temperature. This makes it possible for us to discuss the origin of the ferromagnetism based on the XRD data obtained at room temperature.

Next, we discuss the effects of the crystal defects and particle size on the M_s . Since $\langle \epsilon \rangle$, α , and β are too small to find a clear correlation with M_s , we exclude the contributions of these defects in this case. Although the values of $\langle D_{W-A} \rangle$ are significantly different among the samples, simple correlations between $\langle D_{W-A} \rangle$ and M_s cannot be observed. In contrast, the $\Delta \epsilon$ monotonically correlates with M_s (Fig. 5), i.e., M_s shows nearly linear increase with increasing $\Delta \epsilon$. This strongly indicates that $\Delta \epsilon$ contributes to the appearance of ferromagnetism in the Pd nanoparticles. A positive intercept of $\Delta \epsilon$ ($\sim 0.6\%$) was obtained from the linear fitting. In addition, M_s scarcely shows correlations with $\Delta \epsilon_{100}$ and $\Delta \epsilon_{111}$.

We interpret the contribution of $\Delta \epsilon$ to the ferromagnetism in the following paragraphs. According to the previous computational researches, the ferromagnetic moment possibly arose in the bulk Pd due to positive uniform strains larger than 5%–10% and was not induced by smaller strains.^{7,8,11,12} Thus, we expect that the positive strains of the order of 5%–10% should be necessary for the appearance of ferromagnetism also in Pd nanoparticles. Based on the W-A analyses of standard deviation in the strain distribution in a sample,^{16–18} the larger $\Delta \epsilon$ should result in a higher fraction of largely strained bonds in the nanoparticles because $\langle \epsilon \rangle$ is negligible. Furthermore, since the negative strains are not conducive to the appearance of ferromagnetism, the present correlation between $\Delta \epsilon$ and M_s in the Pd nanoparticles suggests that the part of the positive strains with large amplitude can induce the ferromagnetism. This is qualitatively consistent with the theoretical predictions in the bulk Pd. In the present samples, however, $\Delta \epsilon$ is smaller than 1.34%, and thus the fraction of the bonds with strain greater than $\sim 5\%$ is too low to explain all the ferromagnetic moments, based on the conventional strain mechanism which deals with the effects of lattice expansion in bulk Pd. This discrepancy can be explained by the following speculations. First, strains smaller than $\sim 5\%$ have possibly contributed to the onset of ferromagnetism in the previous researches. Each theoretical re-

search provides different values of lattice expansion for the appearance of ferromagnetism, e.g., 5.3%,¹¹ 5.5%,⁸ 6%,⁷ 10%,¹² and less than 5%.¹⁴ Quantitative determination of exact value is still controversial. Next, the strain-induced ferromagnetism would involve another mechanism that has not been predicted under the assumption of the isotropic and uniform lattice expansions. We claim that $\Delta\epsilon$ probably yields anisotropic strains locally in the crystal lattice. The anisotropic strains change the crystal symmetries in the vicinity of atoms which have anisotropically strained bonds. This may also induce the modification of electronic states and thus the appearance of ferromagnetism. This is in contrast to the isotropic strain which induces magnetic enhancement via the narrowing of the $4d$ band and the change in d - s , p hybridization by the expansion of interatomic distance. Provided that the larger strain breaks the crystal symmetries more extensively, this model should be consistent with the positive correlation between M_s and $\Delta\epsilon$. It is worth noting that the ferromagnetic state was stabilized in Pd with hcp symmetry as shown by Hüger and Osuch¹² and Alexandre *et al.*¹⁴ The fcc structure of the Pd nanoparticle may be easily transformed into the hcp structure because of the resemblance between them, e.g., the stacking faults and twin boundaries, which are built by the stacking of $\{111\}$ close-packed layers in the fcc structure, contain a layer with hexagonal symmetry.¹⁴ Moreover, the experimental results supporting the effects of hcp-like structure were also proposed in Ref. 4, which argued the relation between ferromagnetism and twin boundaries. In the present study, such planar defects cannot be evaluated relevant to the ferromagnetism because the amount of the planar defects is insufficiently small to discuss their contribution in our samples. However, in the basis of above discussion, these defects probably induce ferromagnetism in Pd.

In the present experiment, the $\Delta\epsilon$ of 0.5% was the minimum value at which the small M_s was still observed. On the

other hand, the threshold value of $\Delta\epsilon$ ($\sim 0.6\%$) was suggested from the linear fitting in Fig. 5. Now, it remains to be elucidated whether or not the internal ferromagnetism disappears in the sample with smaller $\Delta\epsilon$. If the disappearance of the ferromagnetism with smaller $\Delta\epsilon$ is assumed, M_s appears, when the fraction of the positively strained bond exceeds a certain level. This indicates that the strains are not independent and contribute to the ferromagnetism jointly. In this research, we do not conclude which model is appropriate. However, the nearly linear correlation between M_s and $\Delta\epsilon$ and the threshold value of $\Delta\epsilon$ suggests the possibility of the joint effect of strains.

IV. CONCLUSION

The ferromagnetism in the core region of Pd nanoparticles was studied. In consequence of the W-A analysis of the XRD profile and magnetic measurement, we found a positive correlation between M_s and $\Delta\epsilon$ in the samples. This shows that the strains yield the internal ferromagnetism. This confirms that the origin of the internal ferromagnetism is strains. However, the value of the strain estimated from W-A analysis is insufficient to explain the appearance of ferromagnetism based on previous computational studies. This suggests the indirect contribution of strain such as the effect of changes in crystal symmetry, similar to planar defects.

ACKNOWLEDGMENTS

We would like to thank J. Suzuki and T. Oku for stimulating discussions. Y. Kato is also acknowledged for his help with XRD measurements. This work was supported by the Grant-in-Aid for Scientific Research Program (Grant No. 19310077) from the Ministry of Education, Science, Sports and Culture of Japan.

*Corresponding author; oba@az.appi.keio.ac.jp

¹T. Taniyama, E. Ohta, and T. Sato, *Europhys. Lett.* **38**, 195 (1997).

²T. Shinohara, T. Sato, and T. Taniyama, *Phys. Rev. Lett.* **91**, 197201 (2003).

³T. Shinohara, T. Sato, and T. Taniyama, *J. Magn. Magn. Mater.* **272-276**, e1181 (2004).

⁴B. Sampedro, P. Crespo, A. Hernando, R. Litrán, J. C. Sánchez López, C. López Cartes, A. Fernandez, J. Ramírez, J. González Calbet, and M. Vallet, *Phys. Rev. Lett.* **91**, 237203 (2003).

⁵P. Crespo, R. Litrán, T. C. Rojas, M. Multigner, J. M. de la Fuente, J. C. Sánchez-López, M. A. García, A. Hernando, S. Penadés, and A. Fernández, *Phys. Rev. Lett.* **93**, 087204 (2004).

⁶H. Hori, T. Teranishi, Y. Nakae, Y. Seino, M. Miyake, and S. Yamada, *Phys. Lett. A* **263**, 406 (1999).

⁷V. L. Moruzzi and P. M. Marcus, *Phys. Rev. B* **39**, 471 (1989).

⁸H. Chen, N. E. Brener, and J. Callaway, *Phys. Rev. B* **40**, 1443 (1989).

⁹Y. Oba, T. Sato, and T. Shinohara, *e-J. Surf. Sci. Nanotechnol.* **4**, 439 (2006).

¹⁰V. Kumar and Y. Kawazoe, *Phys. Rev. B* **66**, 144413 (2002).

¹¹L. Vitos, B. Johansson, and J. Kollár, *Phys. Rev. B* **62**, R11957 (2000).

¹²E. Hüger and K. Osuch, *Europhys. Lett.* **63**, 90 (2003).

¹³F. Aguilera-Granja, J. M. Montejano-Carrizales, and A. Vega, *Solid State Commun.* **133**, 573 (2005).

¹⁴S. S. Alexandre, E. Anglada, J. M. Soler, and F. Yndurain, *Phys. Rev. B* **74**, 054405 (2006).

¹⁵N. Takano, T. Kai, K. Shiiki, and F. Terasaki, *Solid State Commun.* **97**, 153 (1996).

¹⁶B. E. Warren and B. L. Averbach, *J. Appl. Phys.* **21**, 595 (1950).

¹⁷B. E. Warren and B. L. Averbach, *J. Appl. Phys.* **23**, 497 (1952).

¹⁸C. E. Krill, R. Haberkorn, and R. Birringer, in *Handbook of Nanostructured Materials and Nanotechnology*, edited by H. S. Nalwa (Academic, New York, 2000), Chap. 3, p. 155.

¹⁹B. E. Warren and E. P. Warekois, *Acta Metall.* **3**, 473 (1955).

²⁰S. Ino, *J. Phys. Soc. Jpn.* **27**, 941 (1969).

²¹T. Hayashi, T. Ohno, S. Yatsuya, and R. Uyeda, *Jpn. J. Appl. Phys.* **16**, 705 (1977).

²²K. Reimann and R. Würschum, *J. Appl. Phys.* **81**, 7186 (1997).